Real-Time Control of a PRV in Water Distribution Networks for Pressure Regulation: Theoretical Framework and Laboratory Experiments

Nicola Fontana, C.Eng., M.ASCE[1]; Maurizio Giugni[2]; Luigi Glielmo[3]; Gustavo Marini, C.Eng., M.ASCE[4]; and Francesca Verrilli[5]

Abstract: Pressure-reducing valves (PRVs) are often used in water distribution networks (WDNs) to regulate pressure for leakage reduction. Optimal management would require the pressure to be constant and as low as possible at the WDN critical node. Such operating conditions can be achieved by means of real-time control (RTC) of the PRVs. Because the pressure RTC of PRVs in WDNs is still an uncommon application, this paper first provides the theoretical framework of control systems and also discusses the benefits of a feedback control over a feedforward scheme. A closed-loop controller was developed, allowing RTC of pressure at the critical node in a WDN by changing the pressure set point in the PRV at the network inlet. To this end, a diaphragm-actuated control valve coupled to an actuator for remote control of the pilot spring was used. Laboratory experiments were carried out to characterize PRV operation and effectiveness of the algorithms. A simplified model of the PRV and numerical simulations to reproduce the pressure transient were also developed. Results show that (1) the algorithm is able to control pressure also in case of abrupt variations of the set point pressure and finite delays; and (2) the numerical model is in good agreement with relevant experiments. **DOI: 10.1061/(ASCE)WR.1943-5452.0000855.**

Author keywords: Water distribution networks; Leakage reduction; Pressure-reducing valve; Real-time control.

Introduction

Pressure-reducing valves (PRVs) are increasingly used for pressure control and leakage reduction in water distribution networks (WDNs). PRVs are usually installed at the inlet of a district meter area (DMA) to reduce pressure levels and consequently water losses across the district. In other cases, PRVs may be deployed within a WDN. Approaches and methodologies to maximize the effectiveness of PRVs have been discussed in the literature, which includes numerous studies aiming at optimizing numbers, locations, and settings of PRVs (Araujo et al. 2006; Liberatore and Sechi 2009; Nicolini and Zovatto 2009).

PRVs are set to minimize pressure over a network while ensuring a minimum pressure at all nodes. From a practical point of view, it is possible to identify one (or even more) critical nodes. At critical nodes, the pressure head should be monitored and kept greater than the minimum value required to fully satisfy the nodal demand. Such nodes can be identified by means of pressure measurements or numerical models, whereas the minimum pressure to be ensured is assessed based on the network characteristics (e.g., building elevation, pipe characteristics, user requirements, etc.). Because PRVs dissipate excess head, pressure regulation can be coupled with hydropower generation by means of turbines or pumps as turbines (PATs). Recent studies (e.g., Fontana et al. 2012; Carravetta et al. 2014; Giugni et al. 2014) have also pointed out the technical and economic feasibility of such an approach.

Because of the head losses within the WDN, static regulation of the PRV is unable to minimize water losses unless the monitored node is located just downstream of the valve. Head losses may vary according to space and time distribution of water demand. Consequently, the set point pressure of the PRV has to account for the head loss between the valve and monitored node (Germanopoulos 1995), which results in excess pressure during night hours and, generally, far from peak hours. In some cases, pressure can be switched to day or night operations, but excess pressure still remains (Gomes et al. 2011). Furthermore, the pressure regulation needs to address unexpected head losses within the WDN (e.g., in case of a mains break or fire hydrant operation). To avoid lack of service, a higher pressure than the minimum required is usually set during normal operation.

As an alternative, real-time control (RTC) of the PRV is able to ensure the optimal pressure level over the network at any time and under any operating condition (Campisano et al. 2010). Whereas remote control of valves, pumps, and other devices has been widely used within supply and distribution systems over the last decades, very few applications have been developed for pressure control in WDNs.

Ulanicki et al. (2000) investigated methods for planning and implementation of online control strategies. Both predictive and feedback control strategies were developed for areas with many pressure-reducing valves and many target points. Numerical simulations were carried out, confirming that the control strategies allow for achieving leakage reduction close to that predicted by optimal planning studies. Campisano et al. (2010) discussed the

[1]Associate Professor, Dipartimento di Ingegneria, Università degli Studi del Sannio, Piazza Roma 21, 82100 Benevento, Italy.

[2]Professor, Dipartimento di Ingegneria Civile, Università di Napoli Federico II, Edile e Ambientale, Via Claudio 21, 80125 Napoli, Italy.

[3]Professor, Dipartimento di Ingegneria, Università degli Studi del Sannio, Piazza Roma 21, 82100 Benevento, Italy.

[4]Research Associate, Dipartimento di Ingegneria, Università degli Studi del Sannio, Piazza Roma 21, 82100 Benevento, Italy (corresponding author). E-mail: gustavo.marini@unisannio.it

[5]Postdoctoral Researcher, Dipartimento di Ingegneria, Università degli Studi del Sannio, Piazza Roma 21, 82100 Benevento, Italy.

Note. This manuscript was submitted on November 29, 2016; approved on June 14, 2017; published online on October 26, 2017. Discussion period open until March 26, 2018; separate discussions must be submitted for individual papers. This paper is part of the ***Journal of Water Resources Planning and Management***, © ASCE, ISSN 0733-9496.

performance of RTC of PRVs in terms of pressure and leakage reduction with respect to uncontrolled conditions. Numerical simulations were carried out by assuming steady-state conditions and a proportional control of the valves.

Campisano et al. (2012) proposed a general method to calibrate the gain factor of a proportional controller for the RTC of a PRV, with numerical simulations carried out to analyze WDN operation and the gain factor calculated by means of a regressive relation. The effectiveness of the proposed method was assessed by comparing results with a previous tuning procedure. Creaco and Franchini (2013) further proposed a new algorithm that predicts the head loss attributable to the valve on the basis of the pressure head at the monitored node and discharge running the pipe where the valve is installed. Berardi et al. (2015) pointed out the advantages of remote RTC over local RTC in terms of pressure and water-loss reduction. Diaz Vela (2014) proposed a methodology for pressure control in WDNs that integrates the network model, a simplified valve dynamics model, and a stochastic demand model.

Recently, Campisano et al. (2016) proposed a field-oriented methodology for implementing RTC for leakage reduction in a WDN wherein numerical simulations performed on a Norwegian WDN showed the benefit of the control in terms of leakage reduction under different scenarios. Fontana et al. (2016) discussed the RTC of a prototype for both pressure regulation and hydropower generation through laboratory experiments. Needle valves were used, demonstrating great precision in flow and pressure regulation.

In all the aforementioned studies, steady-state conditions were considered, i.e., a very slow movement of the valve was assumed so as to neglect pressure transients caused by the valve operation. Nevertheless, field and laboratory experiments showed that PRV regulation cannot be represented as a sequence of steady states. Dynamics of the various components have to be taken into account in view of the possible instabilities introduced by the feedback actions. For example, Ulanicki and Skworcow (2014) discussed the violent pressure oscillations at the PRV outlet at low flows, and Meniconi et al. (2015) showed the transient following the regulation of a PRV.

A dynamic model of the PRV is thus required in cases of RTC. Although Prescott and Ulanicki (2003) developed a mathematical model of a PRV, its inherent complexity makes such a model unsuitable for RTC. The appropriate model should be both accurate and simple because it has to be ported to a programmable logic controller (PLC), which actuates the pilot valve for regulation.

The idea of this paper is to control the pressure set point in the PRV based on the pressure readings at a monitored critical node. Consequently, this paper will (1) identify a simplified dynamic model of a PRV; (2) develop an integral (I) algorithm for closed-loop control of the pressure at any given monitored node; and (3) discuss the issues (e.g., stability) arising from RTC of the pressure at a monitored node within a WDN. To this aim, an overview of the simplified dynamic system for this problem is provided, including relevant equations and numerical experiments illustrating the system response to perturbations. The benefits of a feedback control over a feedforward scheme are also discussed. Finally, laboratory experiments to identify the PRV dynamic model and show the accuracy of the algorithms are reported.

Methodological Approach

General Aspects of Controllers

The cause-effect correlations among the various quantities involved in pressure control within a WDN can be described by means of typical control engineering block-scheme language. In such schemes, arrows indicate flows of information, rather than flows of material. The output arrows are related to physical quantities (output), possibly measured, whose dynamic behavior is affected by other quantities (input), possibly actuated and indicated by the input arrows. Plus and minus signs, respectively, indicate whether the corresponding variables are to be added or subtracted (Aström and Murray 2008; Franklin et al. 2015).

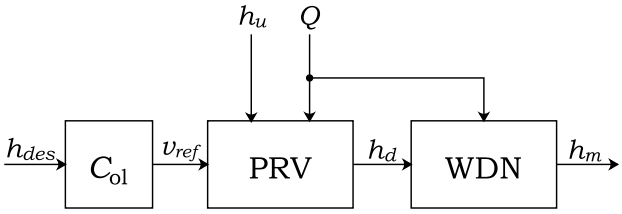

Fig. 1. Open-loop controller of a WDN

For a PRV located at the inlet of a WDN, the block-scheme is given in Fig. 1. Actually, the PRV is a feedback system, with inner feedback loop realized via the hydraulic pilot pipework. Using a simplified representation, the PRV's (information) output is the pressure head h_d downstream of the valve; such pressure may or may not be measured by a transducer, but it is nevertheless relevant to the operation of the WDN.

If a pilot-operated valve is used, an actuator can be coupled to the PRV, which compresses or stretches the pilot spring to vary the pressure set point. The actuator is commanded by an electric signal. Consequently, a one-to-one correspondence can be established between the input voltage and desired output pressure set point, i.e., any desired output pressure set point h_{ref} has a corresponding voltage input to the valve v_{ref}.

From the information standpoint, it is possible to represent the PRV with a block receiving as input the desired voltage v and giving as output h_d (or the head $H_d = h_d + z_{\text{PRV}}$, with z_{PRV} being the PRV elevation).

Other inputs to the PRV should be considered because valve behavior is affected by the flow discharge Q and the pressure h_u upstream of the valve. Although the desired head is a controllable input, i.e., it is set by something or someone upstream, Q and h_u are noncontrollable inputs, i.e., their value cannot be decided by the system. In control engineering, such variables are called disturbance inputs. Furthermore, the PRV is not a simple input-output system with disturbances, but a feedback system itself, with inner feedback loop realized via the hydraulic pilot valve pipework.

In cascade to the PRV, there is the WDN block. The (information) input is the pressure h_d at the valve outlet (i.e., at the network inlet); the output is the pressure at some monitored node h_m. At this node, the head should be kept constant at a desired value h_{des} to both ensure an adequate service level and minimize leakage within the WDN. Such a minimum value can be assessed based on the network characteristics (elevation, topology, discharge, etc.).

It follows that, at least at steady state

$$h_m = f_{\text{ol}}(v; Q) \tag{1}$$

i.e., there exists a relation $v \rightarrow h_d \rightarrow h_m$ parameterized in Q. Such a function can be inverted, at least in principle, so that if one desires the monitored pressure h_m to be equal to h_{des}, the corresponding voltage to be applied to the PRV is given by $v_{\text{ref}} = f_{\text{ol}}^{-1}(h_{\text{des}}; Q)$. In other words, it is possible to choose the reference value for the PRV input as a function, parameterized in Q, of the desired pressure at the monitored node. The controller is a so-called

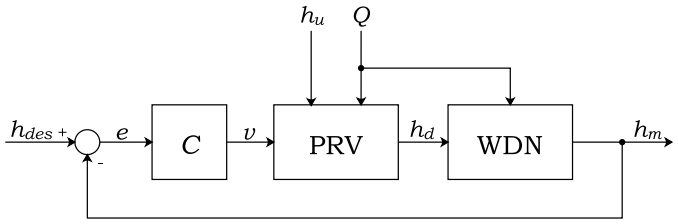

Fig. 2. Closed-loop control scheme

open-loop (or feedforward) controller. The controller C_{ol} in the block scheme of Fig. 1 is the inverse function f_{ol}^{-1}.

Such a strategy, suggested by experience and here mathematically described, is commonly used to control pressure in WDNs. The pressure at the network inlet can also be switched among two or more preselected values, according to the flow discharge Q entering the network in certain day intervals.

The open-loop controller is very simple, only requiring the PRV and (possibly) a scheduler to change the set point (i.e., desired value h_{des}) during the day. Nevertheless (1) such a controller cannot cope effectively with large variations of Q; and (2) determination of the inverse function f_{ol}^{-1} is difficult and uncertain. From a practical viewpoint, f_{ol} has to be calibrated by means of the measurement of flow discharge at the network inlet and pressure in the network (Creaco and Franchini 2013).

An improved controller can be obtained by using information on the actual measured value of $h_m(t)$, thus yielding a feedback (or closed-loop controller). A possible scheme of a feedback controller is given in Fig. 2. In such a controller, the head at the monitored node needs to be measured and transmitted to the computer controlling the system. There, the error $e(t) = h_{\text{des}} - h_m(t)$ becomes the input to the controller C, which computes the input $v(t)$ to the PRV.

In its simplest form, the controller C is a proportional (P) controller because the output is the product of the input e multiplied by some constant gain K_P to be designed. A proportional-integral (PI) controller adds another term given by the integral of the error times a constant K_I (Åström and Murray 2008)

$$v(t) = K_P e(t) + K_I \int_0^t e(\sigma) d\sigma \tag{2}$$

The closed-loop controller thus becomes that shown in Fig. 3.

In Eq. (2), K_P and K_I = proportional and integral gains, respectively. Such gains are tuning parameters, to be set according to the system characteristics. Tuning the gains in a system of many interconnected nonlinear subsystems such as pipes is a very challenging task (Kumar and Kumar 2009). The larger the proportional gain, the larger the change in the controller output for a given error. High

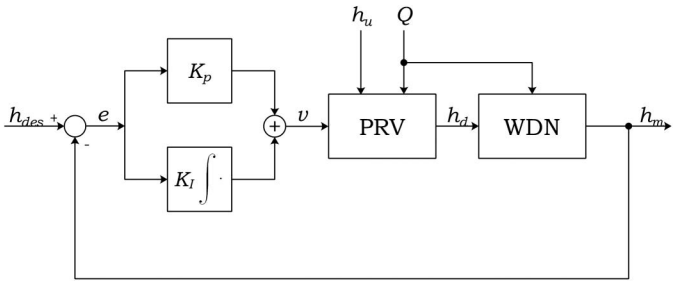

Fig. 3. Closed-loop system with PI controller

proportional gain speeds up the time of response to a disturbance but may cause the system to become unstable. A small gain results in a small output response even to a large error, thus resulting in a less responsive controller. Consequently, low proportional gains may result in ineffective or extremely slow control action when responding to system disturbances. The effect of the integral term in Eq. (2) depends also on the duration of the error; it accounts for the accumulated error, i.e., the larger the accumulated error, the larger the output response of the controller.

To explain the advantage of the PI controller over the simple P controller, assume that a constant reference input $\bar{h}_{\text{des}}$ is applied to the system in Fig. 2. When the system reaches a steady-state condition after occurrence of some transient, a constant input voltage is applied. Denoting the steady-state quantities with a bar, $\bar{e} = 0$ is necessarily obtained. However, $\bar{v} = K_P \bar{e} = 0$ would result if the integral action were not included and the controller were only proportional (i.e., $K_I = 0$). In other words, an error between commanded pressure and output pressure would have to be present in order to generate the control signal (voltage) to set the downstream pressure. A zero error would lead to a zero input voltage regardless of the desired downstream pressure $\bar{h}_{\text{des}}$, whereas an integral controller block can have a nonzero constant output with a zero input (i.e., at steady state). Another way to see this property is the following: if a steady-state is reached, then $\bar{e} = 0$; indeed, if $\bar{e} \neq 0$ occurred at the steady state, the output of the integrator would diverge [Eq. (2)] and bring to divergence $v(t)$, contradicting the steady-state assumption.

The integral term may cause overshooting of the system (Åström and Murray 2008), i.e., a time behavior of the output variable (pressure h_m in this particular case) which surpasses the desired final steady state by some degree before coming back with an undershoot and so on with oscillations. Overshooting may be accepted if the relative extent thereof with respect to the desired step does not exceed some value, which is typically also related to the number of oscillations occurring before settling down.

PRV Dynamic Model

Both open-loop controllers and closed-loop controllers require the behavior of the valve to be known. Furthermore, it is well-known that the dynamic behavior of a PRV cannot be neglected because the output pressure is not able to follow instantaneously abrupt changes in the input voltage and transients occur. The transient following the change of the input setting exhibits different patterns at different values of the flow discharge. At smaller flow discharges, larger oscillations occur. Although a complete model of a PRV is available in the literature (Prescott and Ulanicki 2003; Ulanicki and Skworcow 2014), such a model is unsuitable for RTC. A simpler model is required for real-time operations, and preliminary analysis showed the response of the valve to a step input to be well represented by the step response of a second-order linear model, similar to a mass-spring mechanical behavior. The behavior of many systems is analogous to the behavior of a mass tied using spring and damping elements to a fixed position. The response of such second-order systems depends on the characteristics of their elements. Some are oscillatory and characterized by decaying or (in the ideal no-friction condition) persistent oscillations, whereas others do not exhibit oscillations in their responses because of large damping (e.g., Åström and Murray 2008; Franklin et al. 2015). The canonical form of a second-order system with decaying oscillatory behavior is given by

$$\frac{d^2x(t)}{dt^2} + 2\xi\omega_n \frac{dx(t)}{dt} + \omega_n^2 x(t) = \mu\omega_n^2 u(t) \tag{3}$$

where $u(t)$ = external excitation; dimensionless parameter $\xi \in [0, 1]$ = damping ratio; ω_n (rad/s) = undamped natural frequency; and μ = static gain, i.e., ratio between the steady-state value of the system output and its constant input. For $\xi \in [0, 1)$ the response of system Eq. (3) to a step signal $u(t) = \bar{u}$ for $t \geq 0$ can be written (Franklin et al. 2015)

$$x(t) = \mu\bar{u}\left[1 - \frac{1}{\sqrt{1-\xi^2}} e^{-\xi\omega_n t} \sin\left(\omega_n t\sqrt{1-\xi^2} + \cos^{-1}\xi\right)\right] \quad (4)$$

For $\xi = 0$, the system oscillates persistently at frequency ω_n. At increasing values of ξ (but with $\xi < 1$), the oscillation frequency decreases and the exponential decaying becomes more evident, so that the response goes to a steady state in an increasingly shorter time for progressively larger values of ξ.

Actually, the model Eq. (3) does not take into account the offsets from zero. Indeed, it is straightforward to verify that—provided the system is damped, i.e., $\xi \in (0, 1)$—the steady-state response $\bar{x}$ corresponding to a constant input $u(t) = \bar{u}$ for all t is $\bar{x} = \mu\bar{u}$ [it is easily checked by zeroing the derivatives in Eq. (3) or letting $t \to \infty$ in Eq. (4)]. In other words, the steady-state relation between $\bar{u}$ and $\bar{x}$ is represented by a straight line passing through the zero. This, however, does not apply in the PRV case, as can be seen in the experimental plot of Fig. 7, whose nonsaturated part has an evident offset. The issue is solved by translating the axes around the working point $\bar{u}$, $\bar{x} = \mu\bar{u}$, i.e., setting $x(t) = \bar{x} + \delta x(t)$ and $u(t) = \bar{u} + \delta u(t)$. The resulting outcomes are again Eq. (3) with $\delta u(t)$ replacing $u(t)$ and $\delta x(t)$ replacing $x(t)$.

Stability of a Closed-Loop Controller

Whereas the open-loop controller is technologically simple but could yield slow and imprecise behavior, a feedback action results in a faster and more robust working of the system. Nevertheless, a closed-loop controller presents some additional issues. One of the most important issues is that feedback control can generate oscillations and even instability in the presence of actuator saturation (i.e., the output of the controller, which is an actuation request, goes beyond the design limits of the actuator) and finite delays. When regulating pressure in a WDN, both constraints may occur because (1) the PRV cannot provide more pressure than its upstream head, and (2) the head variation at the monitored node is felt with some finite delay τ because of the finite propagation velocity of pressure waves. Such delay could even amount to several seconds, depending on pipe material and distance between the PRV and the monitored node.

Control theory provides tools to analyze the robustness of a feedback control loop with respect to finite delays. An effective tool is based on the so-called frequency response (Powell and Emami-Naeini 2015). The concept applies to any linear system, but for simplicity's sake, the second-order system described by Eq. (3) is considered. A classical measure of robustness called phase margin will be used in what follows, although different approaches (e.g., the Nyquist plot) can be used if both phase and gain are uncertain.

As shown in greater detail in the Appendix, the steady-state response of a dynamic system subjected to a sinusoidal input is governed by its frequency response. If the system has a feedback loop, the closed-loop frequency response depends on the open-loop frequency response. Problems may arise around the so-called critical frequency ω_c where the loop gain equals 1, i.e.

$$|G(\omega_c)(K_P + K_I/j\omega_c)| = 1 \quad (5)$$

where $G(\omega)$ = frequency response of system Eq. (3).

Indeed, when small values of the distance between the loop gain phase at ω_c (typically negative) and $-180°$ occur, a resonant behavior arises around that frequency, causing persistent oscillations during transient behavior. Such distance is called the phase margin $\varphi_m = \angle[G(\omega_c)(K_P + K_I/j\omega_c)] - (-180°)$. Experience teaches that a φ_m value of approximately 60° is reasonable (D'Azzo and Houpis 1988). Typically, the phase margin decreases when increasing the gains K_P and K_I, and a trade-off has to be found between this aspect and the low-frequency behavior which, as will be seen in the Appendix, demands high gains.

The phase margin can be used to measure robustness of the control loop against a finite delay of duration τ. A delay τ implies a phase delay $\omega\tau$ at frequency ω {because $\sin[\omega(t-\tau)] = \sin(\omega t - \omega\tau)$} and one has just to impose

$$\omega_c\tau \leq \varphi_m \Leftrightarrow \tau \leq \frac{\varphi_m}{\omega_c} = \tau_M \quad (6)$$

Obviously, inequality Eq. (6) can be used in two ways: if the loop gain is decided, in the sense that K_P and K_I have been chosen, one can compute ω_c and the maximum delay τ_M admissible to maintain stability. Conversely, given the delay τ, one can choose the gains (and, consequently, ω_c) so that a safe stability margin is left.

A safe way out of this problem is slowing down the control reactions by choosing smaller values of the gains K_P and K_I, thus yielding a larger phase margin but also a reduction of dynamics performance.

Another possible remedy to finite delays is given by the so called Smith's predictor (Franklin et al. 2015) (Fig. 4). The real WDN (dotted-line box in Fig. 4), it is assumed, can be described by the (information) cascade of an ideal WDN (iWDN), where the pressure transient propagates instantaneously (i.e., with zero delay), with a finite delay block, which delays input signals by τ seconds. If a model of the iWDN is known, it is possible to subtract the delayed (predicted) value from the actual (measured) value and use the iWDN model to predict the value corresponding to the input without delay.

The blocks in the dashed-line box on Line 1 (Fig. 4) represent the physical system (PRV + WDN) affected by the delay, whose output is cancelled out by subtracting the value predicted by the simulated models on Line 2. The final outcome is feeding back to the controller the prediction of future measurement h_{pred} coming out of the iWDN simulated model, which does not include the delay (Line 3). In other words, the feedback quantity h_{pred} is the prediction of the output of the WDN after τ seconds, i.e., if there were no delay.

Laboratory Setup

Experiments were carried out at the Hydraulic Laboratory of the Department of Civil, Architectural, and Environmental Engineering of the University of Naples Federico II in Naples, Italy. The four-loop network described by Fontana et al. (2016) was used for experiments. The network is supplied by a pump, which delivers a flow discharge up to 45 L/s at a maximum pressure head around 70 m. An air chamber is located at the network inlet to avoid pressure and flow fluctuations during experiments.

The network is made of cast iron, with a nominal diameter of 150 mm. Small segments of steel are also used for ease of installation. A total of 19 motorized gate valves were installed for

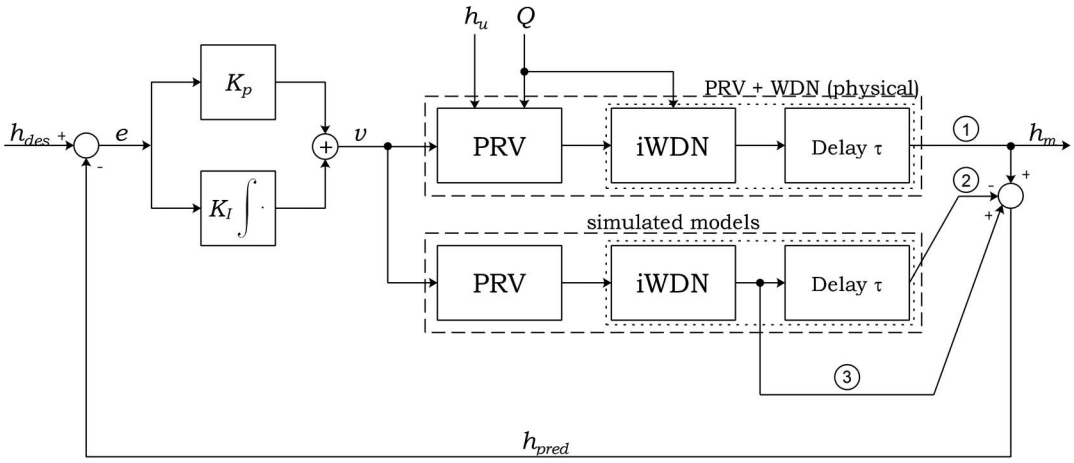

Fig. 4. Smith's predictor scheme to cope with finite delays

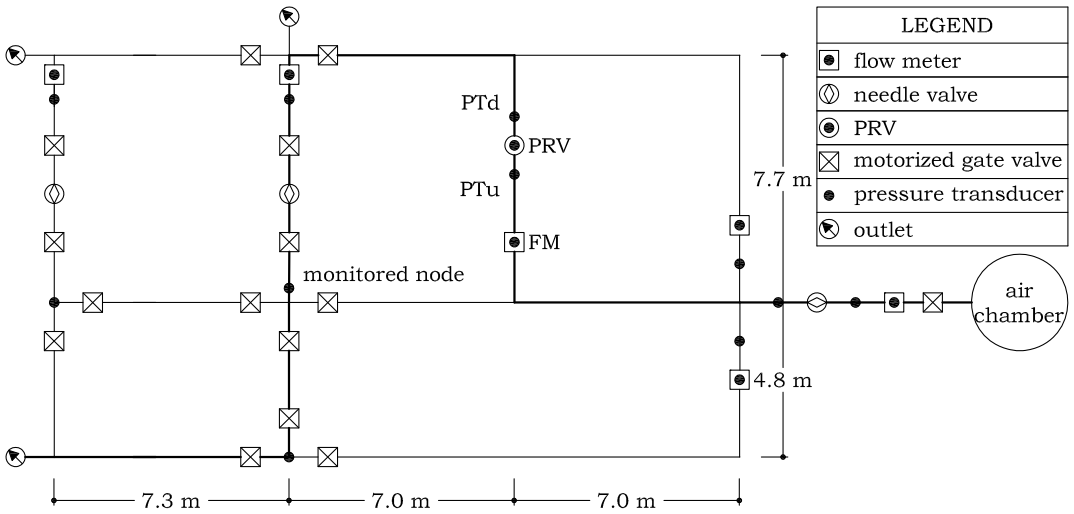

Fig. 5. Sketch of the laboratory network

flow control, actuated with electric actuators for opening and closure. Flow discharge can be regulated by means of manual valves located at three outlets; in addition, 11 pressure transducers and 7 flow meters are also deployed within the network for complete flow characterization. A new pipeline was added to the network where the PRV and a flow meter were installed (Fig. 5). Only the thick line in Fig. 5 was used for experiments. Consequently, some of the motorized gate valves were left closed. Flow discharge was varied by means of the outlet valve at the lower left corner of the network. The PRV is a pilot-operated Bermad valve (BERMAD, Porterville, California), model EN 720 4SE-VI, nominal diameter 150 mm. The valve is hydraulically operated by means of a diaphragm actuator that reduces the upstream pressure to a lower constant downstream pressure. Pressure regulation is independent of upstream pressure and flow discharge. A schematic of the valve is given in Fig. 6.

The needle valve (Point 1) in Fig. 6 enables continuous inflow from valve inlet to the upper control chamber (Point 2). Eventual rises in downstream pressure above the pilot setting induces pilot (Point 3) throttling, causing pressure accumulation in the upper control chamber. The main valve throttles closed, decreasing downstream pressure to the pilot setting. Conversely, upon downstream pressure dropping below pilot setting, accumulated pressure is released by the pilot, with the main valve modulating open.

The steady-state downstream pressure set point is set by the compression of the pilot spring. The greater the spring compression, the lower the outlet-pressure set point. Unlike common PRVs, the valve is equipped with a motorized pilot, i.e., an actuator is mounted on the valve, which compresses or stretches the pilot spring, thus varying the outlet pressure. The actuator is commanded by an input voltage v between 0 and 10 V. Consequently, it is possible to remotely command the outlet-pressure set point of the valve by varying the input voltage. Input voltage of 0 V corresponds to the maximum outlet-pressure set point, whereas an input voltage of 10 V corresponds to the minimum outlet-pressure set point (ideally, closed valve).

A flow meter model G2 PMAG (Asti, Italy) for precise flow measurement was installed (FM in Fig. 5). Two pressure transducers (model WIKA S-11, Klingenberg am Main, Germany), with a pressure range of 0–10 bars and accuracy of 0.25% were also installed, upstream (PTu), and downstream (PTd) of the valve. Data were collected by a PLC and sent to a system control and data acquisition (SCADA) unit for visualization and storage. Sampling

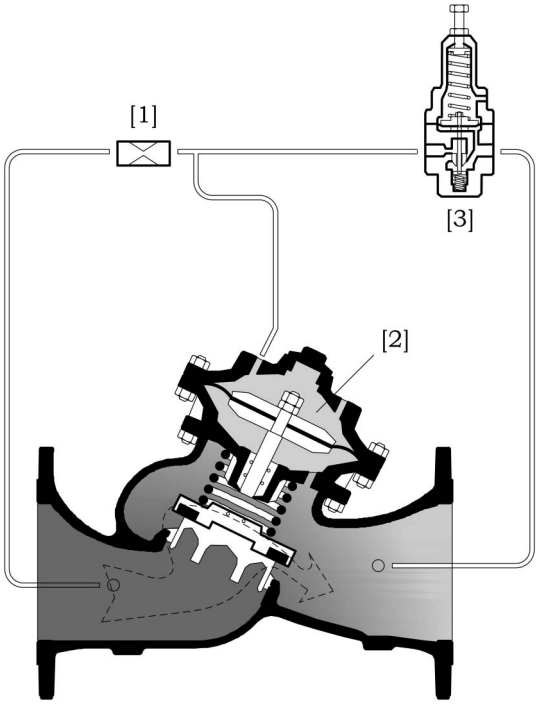

Fig. 6. Schematic of the PRV (adapted from Bermad 2017)

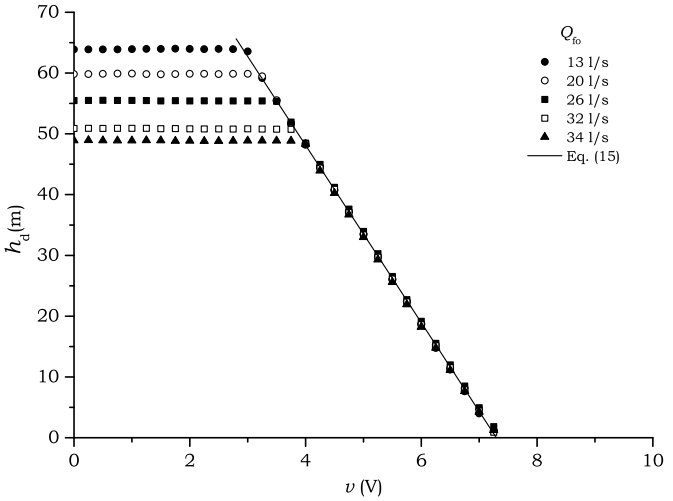

Fig. 7. Pressure at the valve outlet at varying input voltages and flow discharges

interval for data storage was varied between 0.11 and 1 s, depending on the temporal resolution required by the experiment.

Sampling time is another important issue to consider for proper control. Sampling time (and so the time between two successive adjustments of the valve pilot set point) is closely related to the required response time of the controller. For RTC of pressure in WDNs, such time could also be in the order of minutes because of the (generally) slow variation of flow and pressure. In such a case, the design would be much simplified because the dynamics of the valve and the finite delay of the WDN can be ignored.

Accordingly, a static PRV model can be used, and the Smith's predictor can be omitted. A (low-pass) prefiltering of the pressure measurement before sampling is required to capture only the slowly varying component of the signal. Nevertheless, in case of sudden abnormal operation of the WDN (e.g., in case of break of transmission mains or for fire hydrant service), a very long time is required for the controller to adequately set the downstream pressure.

From another viewpoint, sampling time is related to communication infrastructure. In the laboratory rig, PLCs communicate using a wired (Ethernet) connection, which is fully consistent with PLC scan rate (in the order of milliseconds), and control times can be quite small. This means that communication between the remote PLC and the valve PLC is not a crucial issue in a laboratory environment. Contrariwise, in real field installations, the design has to take into account the infrastructure needed to transmit data from measurement points to the controller (i.e., pressure data) and from the controller to the actuator (i.e., PRV input voltage).

Only in rare cases a wired communication can be used, therefore alternatives [e.g., Wi-Fi or Global System for Mobile Communications/General Packet Radio Service (GSM/GPRS) connections] should be considered. The GSM/GPRS connection is currently the most effective solution because there are no limitations in terms of distance and/or visibility between connected points as for a Wi-Fi connection. Consequently, two modems at both the inlet node and the monitored node should be also installed. The modems create a virtual private network (VPN), which allows secure traffic on a public Transmission Control Protocol/Internet Protocol (TCP/IP) network.

If a Point Input/Output (I/O) module is deployed at the monitored node, then the system will work again with very low sampling times, similar to with a wired connection, according to the PLC scan rate. For the used PLCs, the maximum scan time is 750 ms. Alternatively, a PLC should also be deployed at the monitored node. In this case, the control time step of the controller can be set at will. In summary, if smaller time steps are used, the controller is more responsive, although the costs of transmission between valve PLC and remote PLC increase.

Experiments

Steady-State and Transient Models of a PRV

A number of laboratory experiments were carried out to characterize the PRV behavior in order to identify a suitable model to be used in the design and simulation of the various control schemes. Steady-state and transient behaviors of the PRV were identified by varying the controlled pressure at the valve outlet.

Steady-state PRV behavior was characterized at varying inflow discharge Q and upstream pressure head h_u. A number of experiments were run by first setting the initial flow discharge at fully open valve Q_{fo}, then increasing the input voltage v to the PRV (which commands the variation of the pressure at the valve outlet). At the start of each experiment, the input voltage was set to 0 V and then progressively increased by 0.25 V at each step. The voltage was kept constant for 2 min before the next step input in order to achieve steady-state conditions. The experiments were stopped when the downstream pressure was lower than ~1 m. The steady-state pressure head downstream of the valve h_d at varying v and Q is plotted in Fig. 7.

Plotted data show the relation is linear in the interval 3–7 V. For input voltage smaller than ~3 V, no regulation was performed because the commanded pressure would be greater than h_u. In this case, the valve is basically open, and the pressure at the valve outlet is the upstream pressure minus the head loss within the valve, in the order of 3–4 m. Consequently, the outlet pressure is flat as a function of the input voltage. In the experiments, such a constant value varied according to the inflow discharge because of the laboratory

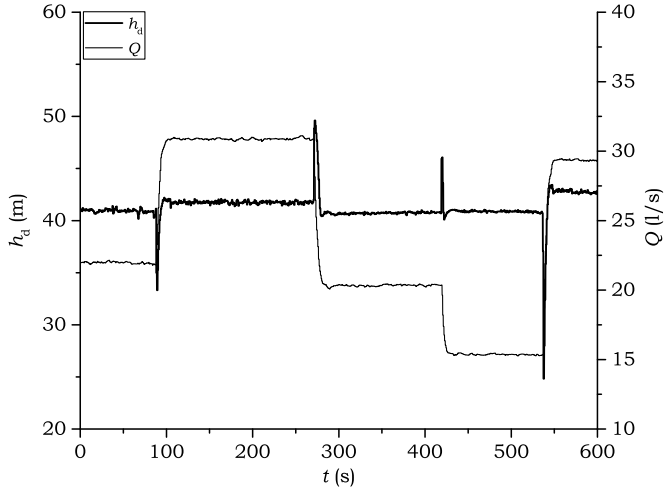

Fig. 8. Pressure at the valve outlet at varying flow discharges

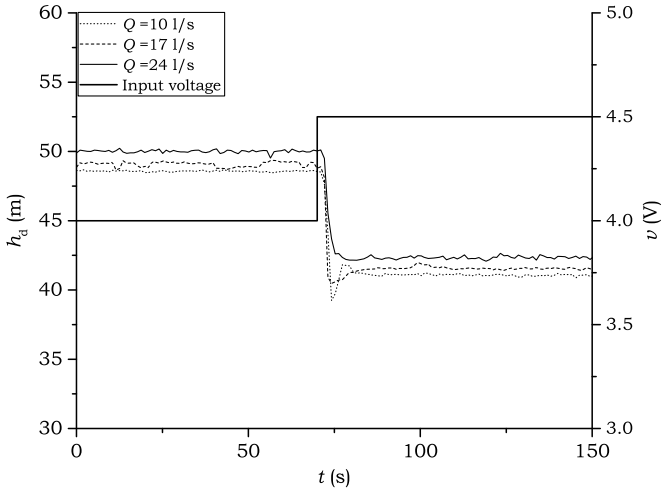

Fig. 9. Pressure at the valve outlet at varying flow discharges and input voltages

circuit supply system. The air chamber at the network inlet (Fig. 5) is supplied by a centrifugal pump. For such pumps, the greater the flow discharge, the smaller the head given by the pump, and hence the upstream pressure h_u.

The following equation was inferred:

$$h_d = -14.60v + 106.5 \tag{7}$$

with a coefficient of correlation of 0.9995, with h_d in meters and v in volts. Nevertheless, experiments showed a certain influence of Q and h_u on the steady-state commanded pressure because of mechanical nonlinearities and hystereses embedded in the PRV operations. Consequently, for the same input voltage, slightly different steady-state pressures at the valve outlet were achieved, depending on the flow characteristics and also on the input voltage step height. As an example, in Fig. 8 the pressure at the valve outlet was plotted at varying flow discharge for a constant input voltage $v = 4.5$ V.

Flow discharge was varied by abrupt operation of the outlet valve. The opening of the outlet valve results in increased flow; consequently, the pressure at the valve outlet suddenly decreases. The valve operates so as to reduce the internal head loss, thus maintaining the pressure at its outlet at a constant value. Similar considerations apply when the outlet valve is closed. Nevertheless, pressure regulation presents some inaccuracies, as mentioned earlier. According to Eq. (7), a steady-state pressure around 41 m was calculated, but differences in the order of 1–2 m occur. Experiments showed that, as a general rule, the greater the flow variation, the greater the difference between the outlet pressure before and after valve operation. Similarly, in Fig. 9 the pressure at the valve outlet following a step in v from 4.0 to 4.5 V was plotted at varying flow discharges. However, the head drop corresponding to the step in input voltage is independent of Q.

Having in mind the modeling uncertainties just discussed, Eq. (7) is a reasonable approximation of the steady-state PRV input-output relation and yields the static gain coefficient $\mu = -14.60$ m/V of Eq. (3). Indeed, one can write $\delta h_d = -14.60\delta v$ around the typical working point of voltage and downstream pressure, thus shifting to the origin the leaning line of Fig. 9. Laboratory experiments were further carried out to calibrate the other coefficients ξ and ω_n of the second-order systems of Eq. (3) which characterize its dynamic behavior. The pressure transient was obtained by giving a step voltage as input to the PRV and observing the

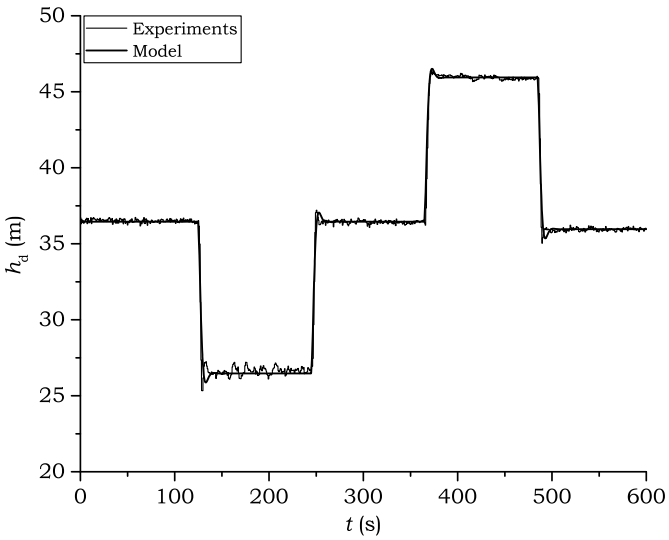

Fig. 10. Experiments and identified PRV model for a sequence of step inputs

output pressure $x(t) = h_d(t)$. The *MATLAB* system identification toolbox [see Ljung (1999) for the methods used therein, and the toolbox documentation for the procedure to be followed] was used for identification.

The following sequence of voltage step inputs was considered for identification: 4.9 to 5.5 to 4.9 to 4.3 to 4.9 V. The results are plotted in Fig. 10, with the identified values of the parameters: $\omega_n = 0.503$ rad/s and $\xi = 0.668$. The details of the pressure transients following the voltage step inputs are given in Fig. 11. The System Identification Toolbox returned a global fit of 94% and values ranging between 85 [Fig. 11(a)] and 89% [Fig. 11(d)] for the time windows of Fig. 11.

Results showed good agreement between experiments and model. Slight differences may be found during some transients, but this behavior is inherent to the use of a simplified model. In any case, both rise time and fall time are fairly well reproduced. For validation purposes, the same parameters were used with a

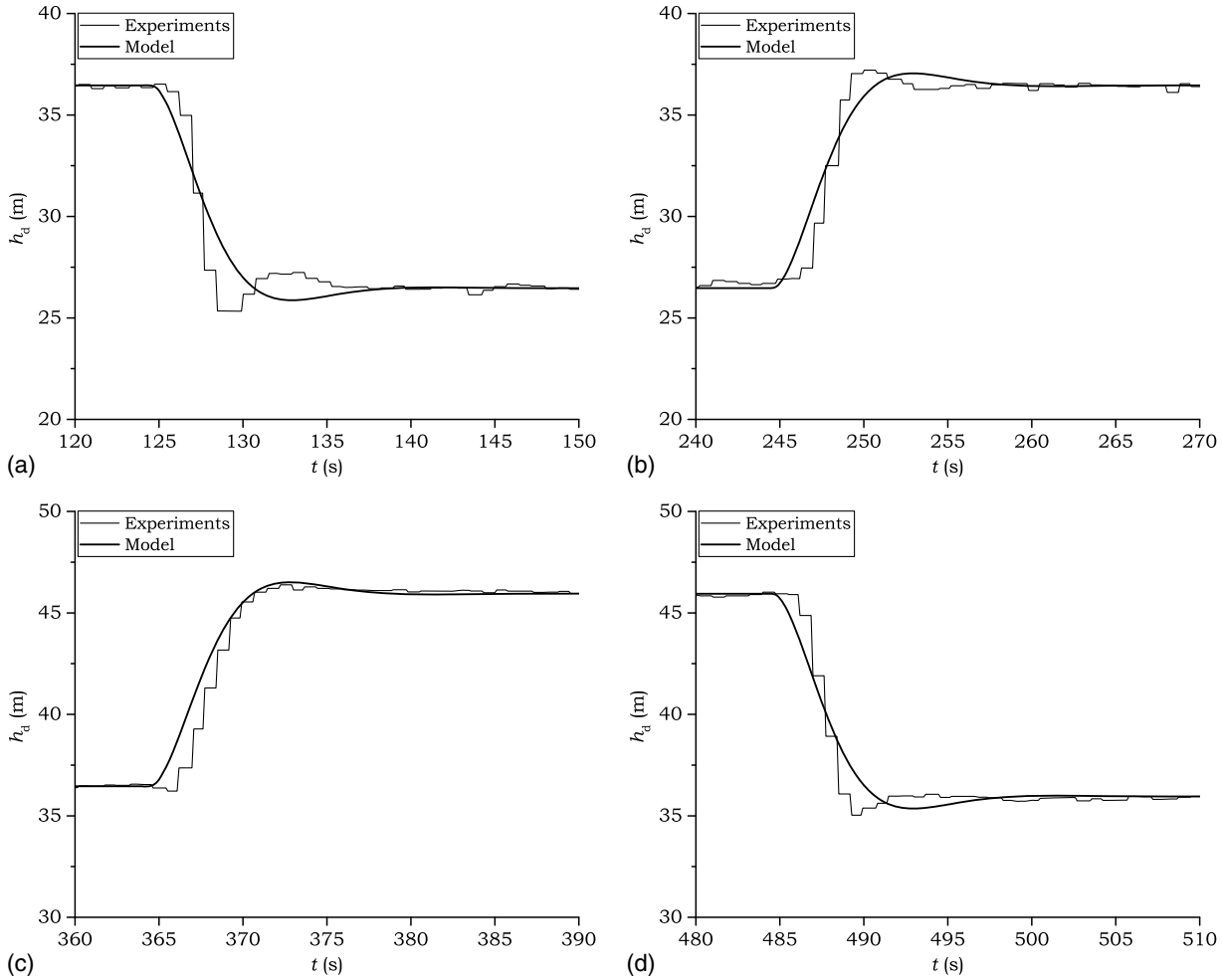

Fig. 11. Details of the pressure transients for a sequence of step inputs

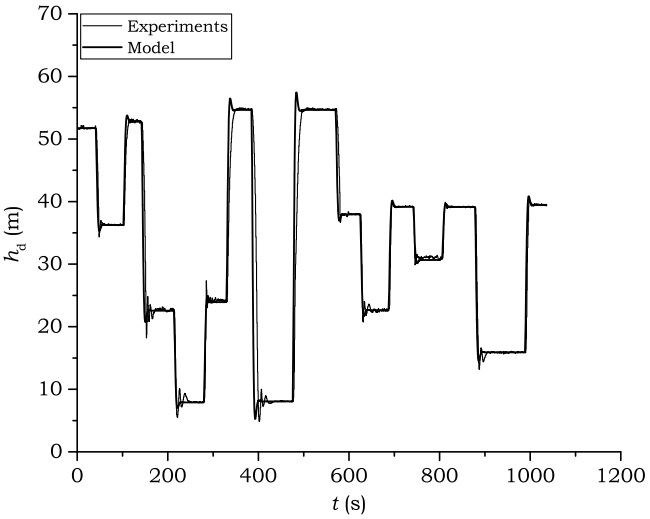

Fig. 12. Validation of the PRV model for different operations

different range of step inputs. Experiments and PRV model were plotted in Fig. 12, and again, they show satisfactory agreement. The greatest differences occur for very large step heights, whereas better agreement was found for smaller pressure drops.

RTC of Pressure in a WDN

In a second phase, experiments were carried out to assess the effectiveness of the algorithms in controlling pressure at the monitored node. Numerical simulations were also developed to compare predicted values with measured values.

Given their lack of robustness against model uncertainties, open-loop controllers were not tested. However, Eq. (7) can be composed with a relation giving the pressure drop across the WDN [e.g., $h_d - h_m = g(Q, z_{\mathrm{PRV}}, z_m)$, with z_m being the elevation of the monitored node], thus obtaining

$$h_m = -14.60v + 106.5 - g \tag{8}$$

i.e., the function f_{ol} of Eq. (1) needed to design an open-loop controller.

Instead, the closed-loop controller of Fig. 2 was used for pressure control. Because of the slow variations of flow and pressure in a WDN, an integral controller (i.e., $K_P = 0$) was considered. The pressure was regulated at the monitored node of Fig. 5. Pressure, flow discharge, and voltage input to the PRV were recorded during the transient so as to characterize control operation.

A first experiment was run by setting the desired head at the monitored node $h_{\mathrm{des}} = 30$ m and varying the flow discharge by opening the outlet valve (Fig. 5). The integrator gain was set to $K_I = -0.005$ V/m · s. The gain has to be negative because of the negative slope of Eq. (7). Results plotted in Fig. 13 show

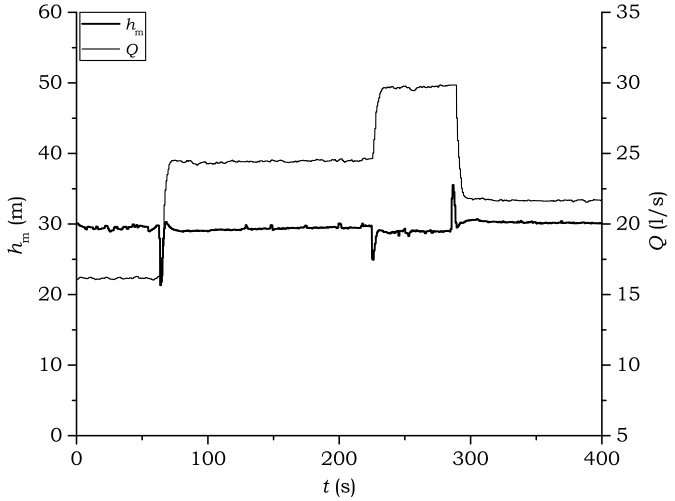

Fig. 13. Pressure control at the monitored node ($h_{des} = 30$ m)

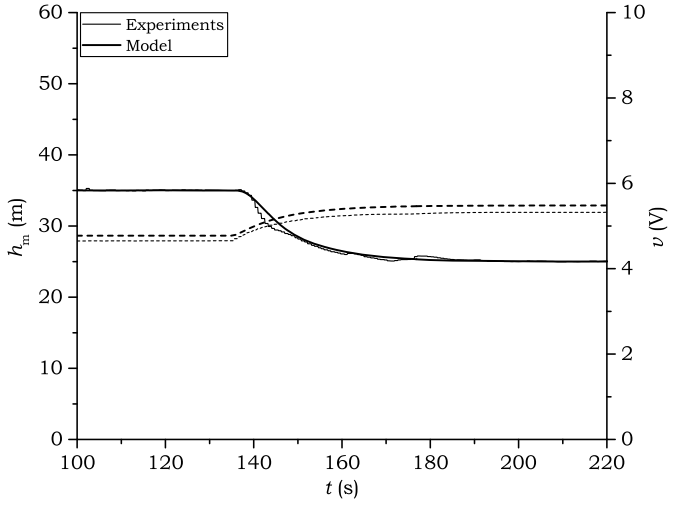

Fig. 14. Pressure transient at the monitored node (continuous line) and input voltage to the PRV (dashed line) during regulation

the ability of the controller to achieve the set point regardless of the inflow discharge.

Although in real environments flow variations are quite smooth, abrupt variations of Q were considered to test the controller in more difficult conditions. Plotted data show the abrupt variation in pressure following the variation in flow, but the valve regulates to restore the desired pressure at its outlet. The controller further regulates the downstream pressure set point so as to achieve the desired pressure at the monitored node.

Because of the small distance between the PRV and the monitored node in the laboratory network, head losses are in the order of a few meters. Only slight regulation of h_d was required to achieve h_{des} at the monitored node. Consequently, further experiments were run to test the reliability of the controller also under extreme operating conditions. The set point pressure was suddenly varied from 35 to 25 m. The integrator gain was set again to $K_I = -5 \times 10^{-3}$. The pressure at the monitored node was plotted in Fig. 14, showing the progressive reduction of pressure until the set point was reached. The transient completed in approximately 60 s, with no oscillation. In Fig. 14, the input voltage to the PRV was plotted

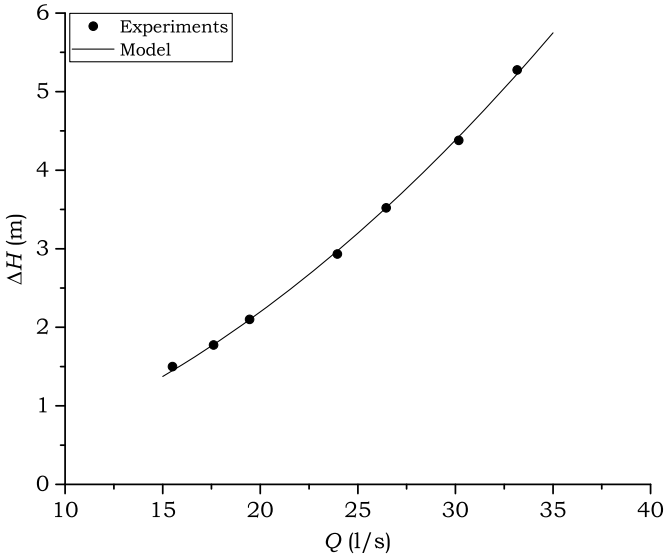

Fig. 15. Head losses between PRV and monitored node at varying flow discharges in the laboratory network

as well, showing the increase of the electric signal sent to the PRV for regulation.

A numerical model was also developed to simulate the controller. Development of a simulation model is quite important when the controller has to be designed for real field applications because of the need to assess suitable values of the control parameters (i.e., gain K_I). The models of both PRV and WDN are required for simulation (Fig. 2). The model of the PRV identified in the previous paragraph was used in the controller.

Regarding the WDN model, a static model was considered because of the small distance between PRV and monitored node (approximately 15 m); thus, inertia effects and finite propagation velocity of pressure waves were neglected. In contrast, in a real WDN, the monitored node can be quite far from the PRV. That results in a larger delay, which cannot be neglected. In this case, a dynamic model of the WDN is required to account for inertia effects, impact of propagation, and reflection of pressure waves.

Nevertheless, because of the complexity of a WDN and the variability of the demand within the network, such a model may result fairly inaccurate in simulating pressure transient. Other factors should be also considered, e.g., time of actuation of the valve and transmission delay. For this reason, concurrent pressure measurements at both the monitored node and downstream of the PRV is the most reliable way to estimate delay.

To develop the model of the laboratory WDN, distributed and concentrated head losses were considered, resulting in a head drop $\Delta H = H_d - H_m$ between PRV outlet and monitored node. In general, head losses mainly depend on the upstream flow Q, but also on network topology, distribution of Q within the network, etc. Because of the simple flow pattern, in the laboratory network, head loss only depend on Q.

Head drop between the valve outlet and monitored node was measured at varying flow discharges (Fig. 15), and an interpolating quadratic relation was inferred from experiments (continuous line in Fig. 15). The outputs of the model were plotted for comparison in Fig. 14, showing the good agreement with experiments during the transient. The modeled input voltage shows an offset with respect to the experimental signal sent to the PRV. This depends on the hysteretic and nonlinear behavior of the PRV (Fig. 9), for which

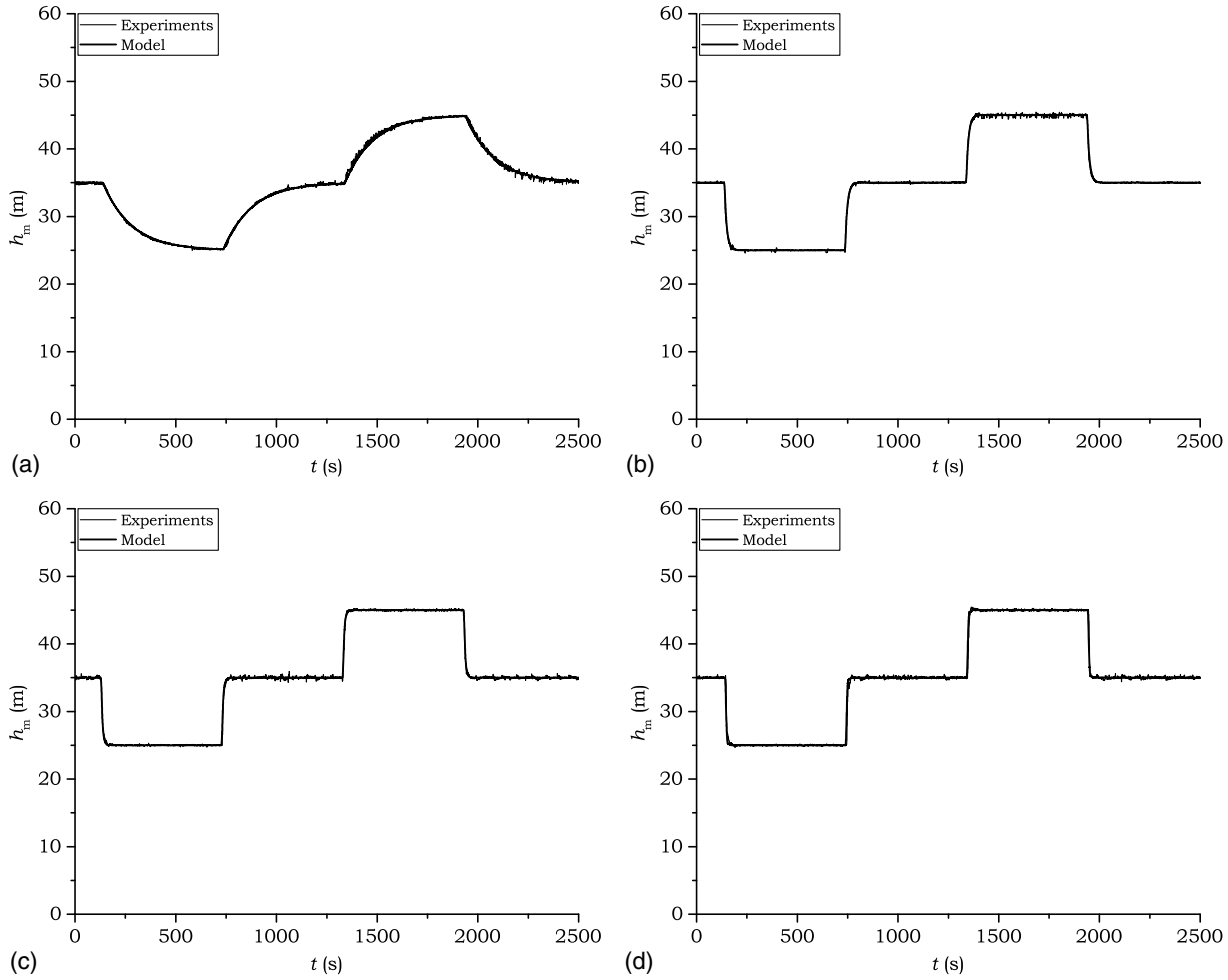

Fig. 16. Closed-loop controller for pressure control at the monitored node for various gains: (a) $K_I = -5 \times 10^{-4}$; (b) $K_I = -5 \times 10^{-3}$; (c) $K_I = -7.5 \times 10^{-3}$; (d) $K_I = -1 \times 10^{-2}$

the same input voltage results in different values of outlet pressure. Precise regulation thus calls for a closed-loop controller rather than an open-loop controller. As mentioned earlier, such an offset is constant, i.e., hysteresis of the PRV, acts mainly on the reference pressure, less so on the variations, especially for slow operations.

Experiments were repeated by setting different values of the gain ($K_I = -5 \times 10^{-4}$, -7.5×10^{-3}, and -1×10^{-2}) to assess response time and regulation stability of the controller upon achieving the set point pressure. The greater the gain, the faster the system reaches the set point pressure, but also the greater the risk of oscillations and instabilities. The set point was set to 25, 35, and 45 m to assess whether (1) the controller is able to regulate the pressure at the monitored node in different operating conditions, and (2) the model reliably predicts the pressure transient at the monitored node. Results are plotted in Figs. 16(a–d). For the sake of simplicity, only the pressure at the monitored node was plotted, showing in all cases good agreement between experiments and model, regardless of the integrator gain.

Experiments were further carried out to assess the effects of time delay on the pressure control. Although such delay could amount to several seconds in real WDNs, it is quite small in the laboratory network, as mentioned earlier. Consequently, time delay was simulated by shifting of τ s the acquisition of measured pressure. A 9-s delay was considered in the experiments.

In Figs. 17(a–d), the pressure measured at the monitored node was plotted with the simulated values. Results again show a good agreement with experiments, especially for small values of the gain. For greater values, differences are more significant, although the model is able to correctly identify the frequency of oscillations. At small values [Fig. 17(a)], the response is quite slow; as expected, the greater the integrator gain, the greater the pressure oscillations and overshooting. In particular, Fig. 17(d) shows undamped oscillations of pressure between the maximum and minimum possible values occurring because of the high gain and finite delay. For greater gains, the model is unable to provide accurate simulation of pressure patterns, which depends on the use of a simplified model for the PRV, a steady-state WDN model, and the linear approximation intrinsic to the model. Nevertheless, the model is able to predict the oscillations frequency and, to some extent, also the amplitude.

Such behavior is consistent with the aforementioned stability analysis. When only the integral action is considered, the critical frequency ω_c can be calculated from the following equation derived from Eq. (18):

$$\frac{K_I \mu}{\omega_c \sqrt{[1 - (\omega_c/\omega_n)^2]^2 + 4\xi^2(\omega_c/\omega_n)^2}} = 1 \tag{9}$$

Results are summarized in Table 1, in which the critical frequency, phase margin, and maximum permitted delay (which does

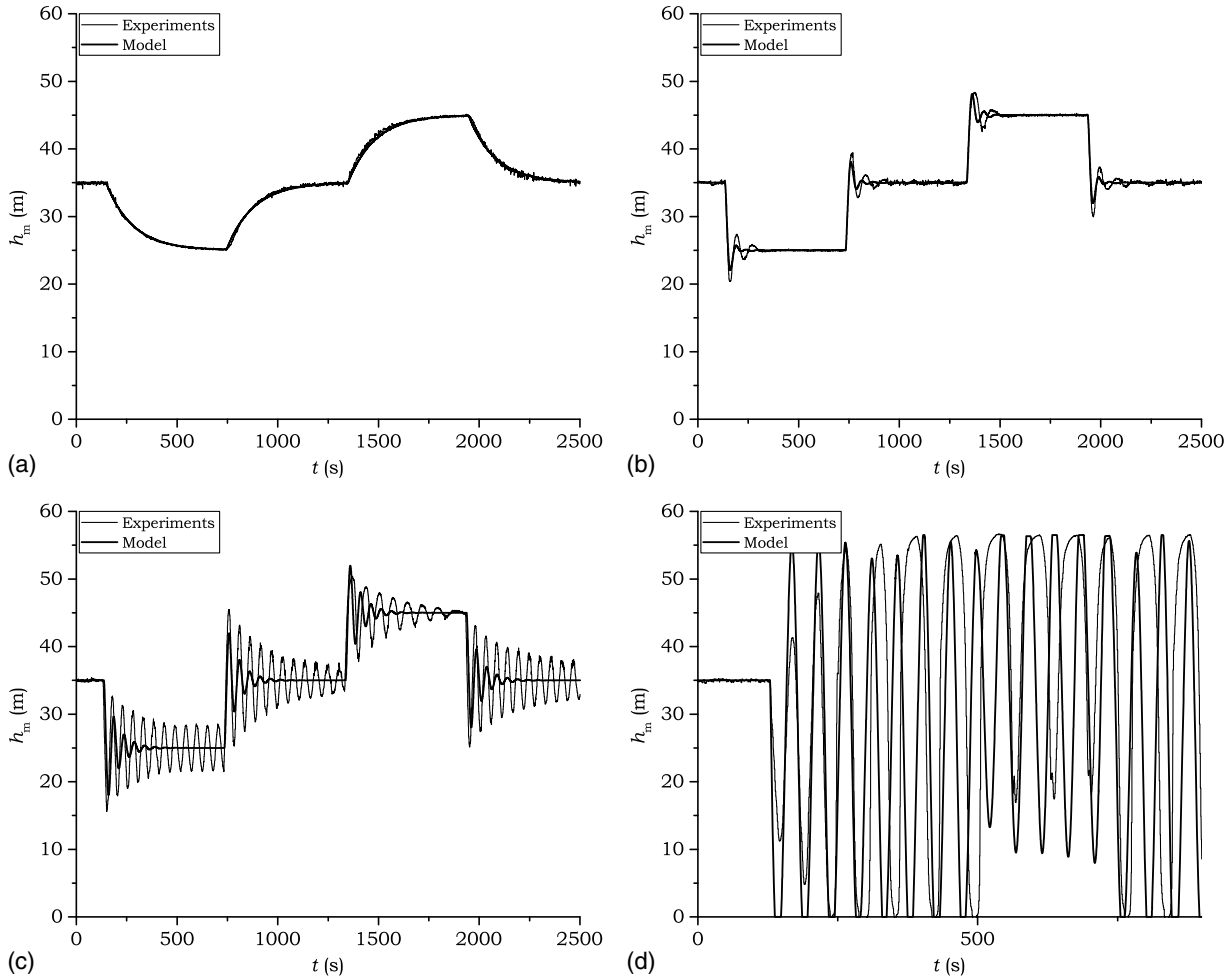

Fig. 17. Closed-loop controller for pressure control at the monitored node for various gains with delay $\tau = 9$ s: (a) $K_I = -5 \times 10^{-4}$; (b) $K_I = -5 \times 10^{-3}$; (c) $K_I = -7.5 \times 10^{-3}$; (d) $K_I = -1 \times 10^{-2}$

Table 1. Critical Frequency, Phase Margin, and Maximum Delay for Various Gains

K_I	ω_c	φ_m	τ_M
−0.0005	0.0073	88.9	212.5
−0.005	0.073	78.8	18.8
−0.0075	0.110	73.0	11.6
−0.01	0.147	66.9	8.0

not lead to instability) for the various integral gains are given. For $K_I = -0.01$, a maximum delay $\tau_M = 8.0$ s was calculated, which is lower than the actual delay ($\tau = 9$ s). Experiments confirmed the unstable behavior of the closed-loop system for such gain value, with undamped oscillations and controller saturation. The maximum delay for $K_I = -0.0075$ is around 12 s, slightly greater than the actual delay. That explains the rise of oscillations, which progressively decay until steady-state conditions are achieved. Conversely, for $K_I = -0.0005$, a greater phase margin is obtained, with a maximum delay of around 200 s, which ensures great stability to the control.

Finally, the results of the controller using the Smith's predictor are given in Figs. 18(a–d). Measured and simulated values exhibit no oscillation, and pressure regulation can be performed with a very regular pattern, similar to with a closed-loop controller without delay. Thus, it is also possible to use higher values of the gain, ensuring a faster response.

Conclusions

Real-time control of the pressure in a water distribution network has been investigated in the paper based on experiments performed on a laboratory network. A closed-loop controller was developed for adjustment of PRV set point pressure to a value such that the pressure at the critical node was equal to the desired pressure. An integral control was used, which ensures no error in regulating the output variable to the set point value at steady state. Pressure was regulated at a monitored node of the network by commanding the outlet pressure of a PRV.

Experiments demonstrated the controller's ability to regulate pressure at the monitored node. Various tests were developed by varying the integrator gain to identify the best trade-off between transient duration and stability of regulation. The experiments also accounted for issues related to transport delays occurring in real environments, showing the oscillations and instabilities that may arise for large gain values. To this end, the effectiveness of a predictor was also assessed.

A simulation model of the entire system, comparing experiments with numerical simulations, was developed. Furthermore, a simplified model of the PRV was identified to represent the valve

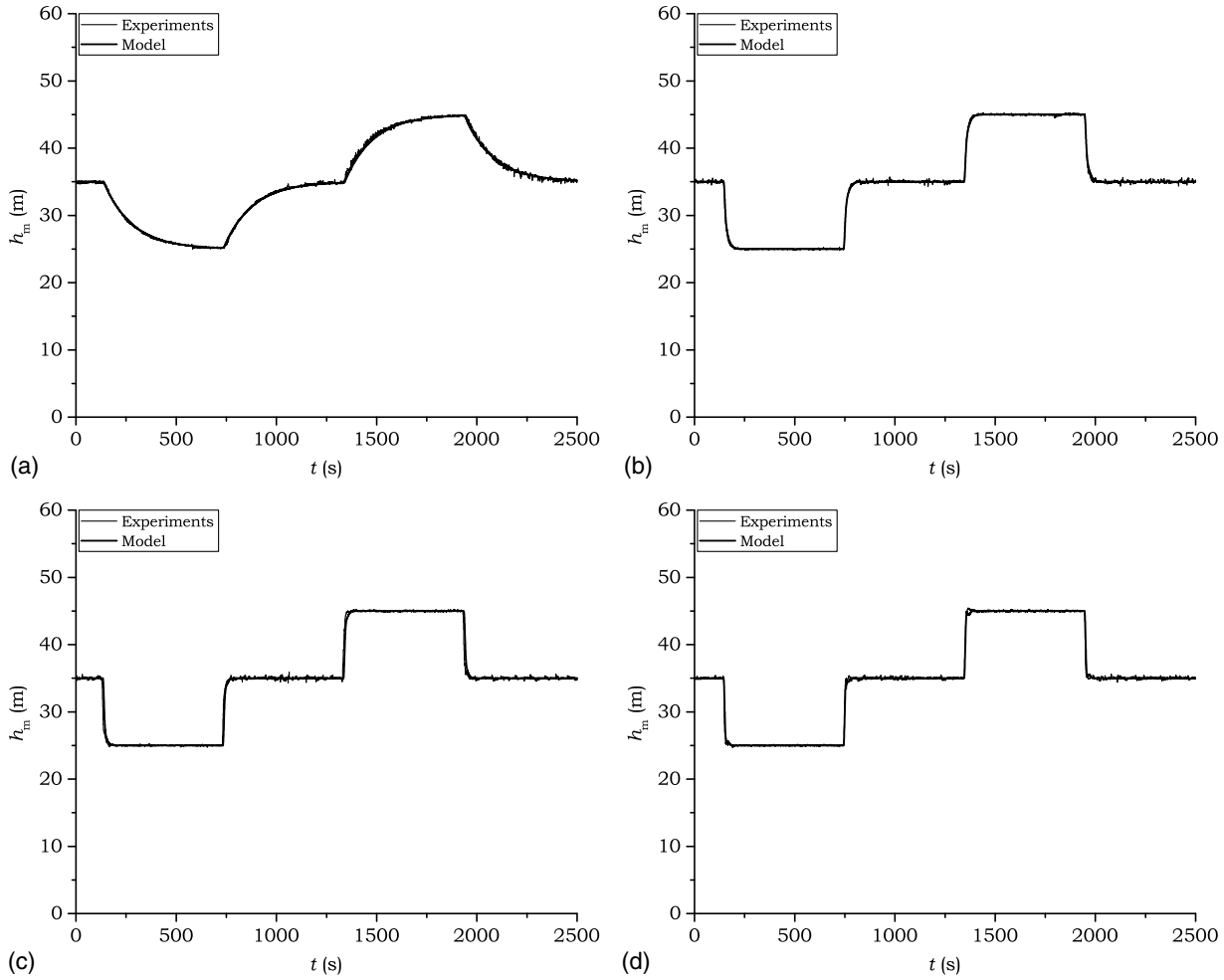

Fig. 18. Closed-loop controller for pressure control at the monitored node for various gains with delay $\tau = 9$ s and Smith's predictor: (a) $K_I = -5 \times 10^{-4}$; (b) $K_I = -5 \times 10^{-3}$; (c) $K_I = -7.5 \times 10^{-3}$; (d) $K_I = -1 \times 10^{-2}$

behavior at varying input settings, as well as a model of the laboratory network. Results showed very good agreement between simulations and experiments, except in cases where transport delay and large integrator gains were considered, owing to the use of simplified models of the PRV and the WDN. Nevertheless, thanks to the slow variations of flow and pressure in WDN, high gains hold less interest from a technical standpoint, besides which, relatively small values yield adequate response to system disturbances.

Appendix. Critical Frequency and Phase Margin for the PI Controller of a Second-Order System

The aim is to compute the steady-state response of the second-order system given by Eq. (3) to the sinusoidal input signal $u(t) = A \sin \omega t = A/2/j(e^{j\omega t} - e^{-j\omega t})$, with j being the imaginary unit, by Euler's formula. Because the system is linear, it enjoys the superposition property, i.e., if one applies the linear combination of some signals as input, the output is the linear combination of the outputs corresponding to each signal. Hence, the steady-state output corresponding to $u(t) = A \sin \omega t$ will be the difference of the outputs corresponding to the inputs $A/2/j(e^{j\omega t})$ and $A/2/j(e^{-j\omega t})$, denoted as $\tilde{u}e^{j\omega t}$ and $\tilde{u}e^{-j\omega t}$ for brevity.

Solutions of the form $x(t) = \tilde{x}e^{j\omega t}$ corresponding to the input $\tilde{u}e^{j\omega t}$ are sought. Because $dx(t)/dt = (j\omega)\tilde{x}e^{j\omega t}$ and $d^2x(t)/dt^2 = (j\omega)^2\tilde{x}e^{j\omega t}$, Eq. (3) becomes

$$[(j\omega)^2 + 2\xi\omega_n(j\omega) + \omega_n^2]\tilde{x}e^{j\omega t} = \mu\omega_n^2\tilde{u}e^{j\omega t} \tag{10}$$

Eq. (10) yields

$$\tilde{x} = G(\omega)\tilde{u} \tag{11}$$

where the complex-valued function

$$G(\omega) = \frac{\mu}{(j\omega/\omega_n)^2 + 2\xi(j\omega/\omega_n) + 1} \tag{12}$$

is the frequency response of system Eq. (3), representing how the behavior of the system changes depending on the frequency of the input signal. The dynamical behavior of the differential Eq. (3) is expressed in Eq. (11) by an algebraic relation where time t does not appear. This turns out to be convenient for analysis and design, as shown next.

The function $G(\omega)$ can be rewritten in polar form, i.e., $G(\omega) = M(\omega)e^{j\phi(\omega)}$ with

$$M(\omega) = |G(\omega)| = \frac{\mu}{\sqrt{[1 - (\omega/\omega_n)^2]^2 + 4\xi^2(\omega/\omega_n)^2}} \tag{13a}$$

$$\phi(\omega) = \angle G(\omega) = -\tan^{-1}\frac{2\xi(\omega/\omega_n)}{1 - (\omega/\omega_n)^2} \tag{13b}$$

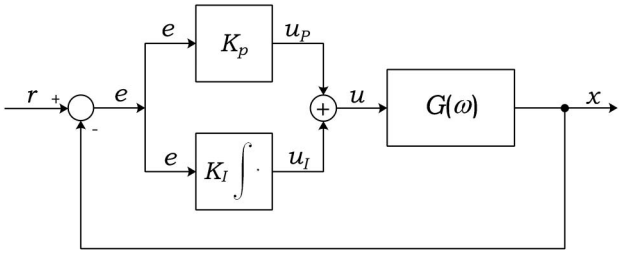

Fig. 19. Closing the loop around a frequency response

where $\angle g$ = phase of the complex number g, and, for simplicity, $\mu > 0$ is assumed; otherwise, the phase would be shifted by 180°. Consequently, one can write

$$x(t) = \tilde{x}e^{j\omega t} = G(\omega)\tilde{u}e^{j\omega t} = M(\omega)\tilde{u}e^{j[\omega t+\phi(\omega)]} \tag{14}$$

The complex sinusoidal function of frequency ω applied as input determines an output given again by a complex sinusoidal function of the same frequency whose amplitude is multiplied by $M(\omega)$ and whose phase is shifted by $\phi(\omega)$. Actually, the signal represented by Eq. (14) is the steady-state response to the complex sinusoidal input. A transient overlaps the steady-state dynamics, but it exponentially decays for asymptotically stable systems, as in Eq. (3). Using superposition, it is straightforward to show that the (steady-state) response to the real sinusoidal input $A\sin\omega t$ is given by

$$M(\omega)A\sin[\omega t + \phi(\omega)] \tag{15}$$

i.e., it is again a sinusoidal signal of the same frequency, with magnitude multiplied by $M(\omega)$ and phase-shifted by $\phi(\omega)$.

Now suppose a feedback loop is closed around the system described by the frequency response $G(\omega)$ as in Fig. 19 with the goal to regulate the output x at the set point r using a PI controller (Fig. 3). Three blocks are in the scheme: (1) the block of frequency response $G(\omega)$; (2) the proportional block; and (3) the integrator block. The proportional block is governed by the algebraic relation $u_p(t) = K_P e(t)$; the integrator block is governed by the equation $du_I(t)/dt = K_I e(t)$, where K_P and K_I are design parameters. Assuming sinusoidal signal and using the procedure seen before, it is readily seen that the frequency response of the proportional block and integrator block are, respectively, K_P and $K_I/j\omega$.

To use the frequency-response tool, a sinusoidal signal r is applied as input, and let x be the system output. Similar to the block scheme of Fig. 2, the error $e = r - x$ is the difference between the system input and output. By using the algebraic representation of frequency response

$$\begin{aligned}\tilde{x} &= G(\omega)\tilde{u} = G(\omega)[(K_P + K_I/j\omega)\tilde{e}] \\ &= G(\omega)(K_P + K_I/j\omega)(\tilde{r} - \tilde{x})\end{aligned} \tag{16}$$

It follows that

$$\tilde{x} = \frac{G(\omega)(K_P + K_I/j\omega)}{1 + G(\omega)(K_P + K_I/j\omega)}\tilde{r} = T(\omega)\tilde{r} \tag{17}$$

where $T(\omega)$ = closed-loop frequency response.

Various aspects are summarized in fundamental Eq. (17). Because the goal of the feedback loop is to make the output x as close as possible to input r (i.e., $e = 0$), $T(\omega)$ has to be as close as possible to 1. For example, if the integrator is not used, i.e., $K_I = 0$, then K_P is chosen to be as large as possible. This choice works well at low frequencies, which are of greater interest for operations [a constant input is just a (phase-shifted) sinusoidal input at zero frequency]. This requirement is often stated as the need for a large loop gain $G(\omega)K_P$ at low frequencies. If the integrator is used, i.e., $K_I \neq 0$, one easily realizes that $T(\omega) \to 1$ for $\omega \to 0$: one gets a precise regulation of the output for constant inputs, a property already discussed in the "Stability of a Closed-Loop Controller" section in a different way.

The loop gain tends to decrease at higher frequencies [as determined from Eq. (13*a*)] so that the (complex) denominator of Eq. (17) may get close to zero at some frequency. This generates a resonant behavior upon excitation at that frequency and, more generally, persistent oscillations, at that frequency, during transients. In addition, $G(\omega)(K_P + K_I/j\omega) = -1$ means $|G(\omega)(K_P + K_I/j\omega)| = 1$ and $\angle[G(\omega)(K_P + K_I/j\omega)] = -180°$. Hence, one way to check the distance from such a situation is to first compute the frequency ω_c at which the loop-gain modulus is 1, i.e.

$$|G(\omega_c)(K_P + K_I/j\omega_c)| = 1 \tag{18}$$

where ω_c= critical frequency and depends on the choices of K_P and K_I. Secondly, the phase $\angle[G(\omega_c)(K_P + K_I/j\omega_c)]$ is computed to check how close it is to −180°. A phase margin $\varphi_m = \angle[G(\omega_c)(K_P + K_I/j\omega_c)] - (-180°)$ of at least 60° is typically specified.

References

Araujo, L., Ramos, H., and Coelho, S. (2006). "Pressure control for leakage minimisation in water distribution systems management." *Water Resour. Manage.*, 20(1), 133–149.

Aström, K. J., and Murray, R. M. (2008). *Feedback systems: An introduction for scientists and engineers*, Princeton University Press, Princeton, NJ.

Berardi, L., Laucelli, D., Ugarelli, R., and Giustolisi, O. (2015). "Leakage management: Planning remote real time controlled pressure reduction in Oppegård Municipality." *Procedia Eng.*, 119, 72–81.

Bermad. (2017). "Bermad waterworks. Hydraulic control valves 700–800 series." Porterville, CA.

Campisano, A., Creaco, E., and Modica, C. (2010). "RTC of valves for leakage reduction in water supply networks." *J. Water Resour. Plann. Manage.*, 10.1061/(ASCE)0733-9496(2010)136:1(138), 138–141.

Campisano, A., Modica, C., Reitano, S., Ugarelli, R., and Bagherian, S. (2016). "Field-oriented methodology for real-time pressure control to reduce leakage in water distribution networks." *J. Water Resour. Plann. Manage.*, 10.1061/(ASCE)WR.1943-5452.0000697, 04016057.

Campisano, A., Modica, C., and Vetrano, L. (2012). "Calibration of proportional controllers for the RTC of pressures to reduce leakage in water distribution networks." *J. Water Resour. Plann. Manage.*, 10.1061/(ASCE)WR.1943-5452.0000197, 377–384.

Carravetta, A., Fecarotta, O., Sinagra, M., and Tucciarelli, T. (2014). "Cost-benefit analysis for hydropower production in water distribution by a pump as turbine." *J. Water Resour. Plann. Manage.*, 10.1061/(ASCE)WR.1943-5452.0000384, 04014002.

Creaco, E., and Franchini, M. (2013). "A new algorithm for real-time pressure control in water distribution networks." *Water Sci. Technol.*, 13(4), 875–882.

D'Azzo, J., and Houpis, C. (1988). *Linear control system analysis and design: Conventional and modern*, McGraw-Hill, London.

Diaz Vela, D. (2014). "Simulation methodology with control approach for water distribution networks." *Proc., Advances in Environmental Sciences, Development and Chemistry*, Inase Press, Montclair, NJ, 37–45.

Fontana, N., Giugni, M., Glielmo, L., and Marini, G. (2016). "Real time control of a prototype for pressure regulation and energy production in water distribution networks." *J. Water Resour. Plann. Manage.*, 10.1061/(ASCE)WR.1943-5452.0000651, 04016015.

Fontana, N., Giugni, M., and Portolano, D. (2012). "Losses reduction and energy production in water-distribution networks." *J. Water*

Resour. Plann. Manage., 10.1061/(ASCE)WR.1943-5452.0000179, 237–244.
Franklin, G. F., Powell, D. J., and Emami-Naeini, A. (2015). *Feedback control of dynamic systems*, 7th Ed., Pearson, Boston.
Germanopoulos, G. (1995). "Valve control regulation for reducing leakage." *Improving efficiency and reliability in water distribution systems*, Springer, Dordrecht, Netherlands, 165–188.
Giugni, M., Fontana, N., and Ranucci, A. (2014). "Optimal location of PRVs and turbines in water distribution systems." *J. Water Resour. Plann. Manage.*, 10.1061/(ASCE)WR.1943-5452.0000418, 06014004.
Gomes, R., Marques, A. S., and Sousa, J. (2011). "Estimation of the benefits yielded by pressure management in water distribution systems." *Urban Water J.*, 8(2), 65–77.
Kumar, M. P., and Kumar, M. S. M. (2009). "Tuning of PID controllers for water networks—Different approaches." *J. Am. Water Works Assoc.*, 101(7), 95–107.
Liberatore, S., and Sechi, G. M. (2009). "Location and calibration of valves in water distribution networks using a scatter-search meta-heuristic approach." *Water Resour. Manage.*, 23(8), 1479–1495.
Ljung, L. (1999). *System identification: Theory for the user*, Prentice Hall, Upper Saddle River, NJ.
MATLAB [Computer software]. MathWorks, Natick, MA.
Meniconi, S., Brunone, B., Ferrante, M., Mazzetti, E., Laucelli, D., and Borta, G. (2015). "Transient effects of self-adjustment of pressure reducing valves." *Procedia Eng.*, 119, 1030–1038.
Nicolini, M., and Zovatto, L. (2009). "Optimal location and control of pressure reducing valves in water networks." *J. Water Resour. Plann. Manage.*, 10.1061/(ASCE)0733-9496(2009)135:3(178), 178–187.
Powell, J., and Emami-Naeini, A. (2015). "Classical frequency-domain design methods." *Encyclopedia of systems and control*, Springer, London, 111–116.
Prescott, S. L., and Ulanicki, B. (2003). "Dynamic modeling of pressure reducing valves." *J. Hydraul. Eng.*, 10.1061/(ASCE)0733-9429(2003)129:10(804), 804–812.
Ulanicki, B., Bounds, P. L. M., Rance, J. P., and Reynolds, L. (2000). "Open and closed loop pressure control for leakage reduction." *Urban Water*, 2(2), 105–114.
Ulanicki, B., and Skworcow, P. (2014). "Why PRVs tends to oscillate at low flows." *Procedia Eng.*, 89, 378–385.